N/P-Codoped Thermally Reduced Graphene for High-Performance Supercapacitor Applications

ARTICLE *in* THE JOURNAL OF PHYSICAL CHEMISTRY C · JULY 2013

Impact Factor: 4.77 · DOI: 10.1021/jp4015959

7 AUTHORS, INCLUDING:

Chunlei Wang
Dalian University of Technology
15 PUBLICATIONS **134** CITATIONS
SEE PROFILE

Ying Zhou
Dalian University of Technology
11 PUBLICATIONS **199** CITATIONS
SEE PROFILE

Jie Shan Qiu
Dalian University of Technology
434 PUBLICATIONS **7,270** CITATIONS
SEE PROFILE

THE JOURNAL OF PHYSICAL CHEMISTRY C

Article

pubs.acs.org/JPCC

N/P-Codoped Thermally Reduced Graphene for High-Performance Supercapacitor Applications

Chunlei Wang, Ying Zhou, Li Sun, Qiang Zhao, Xu Zhang, Peng Wan, and Jieshan Qiu*

Carbon Research Laboratory, Liaoning Key Lab for Energy Materials and Chemical Engineering, State Key Lab of Fine Chemicals, School of Chemical Engineering, Dalian University of Technology, Dalian 116024, China

Supporting Information

ABSTRACT: Graphene relative materials for supercapacitors have incurred intense interest due to their high electrical and thermal conductivity, large surface area, and good chemical stability. N/P-codoped thermally reduced graphene oxide (N/P-TRGO) with high density of surface groups was synthesized by a simple way through thermal annealing of thermally exfoliated graphene oxide in the presence of $(NH_4)_3PO_4$. The extreme low C/O atom ratio of 5.9 was reached after thermal treatment at high temperature of 800 °C for 2 h. N/P-TRGO exhibits high specific capacitance, high rate capability, and excellent cycle performance. The effect of codoping on the surface, structural, and electrochemical capacitive properties was investigated and elucidated in detail. These results demonstrated that N, P codoping is a convenient and efficient way for the improving the supercapacitive performance of thermally reduced graphene oxides.

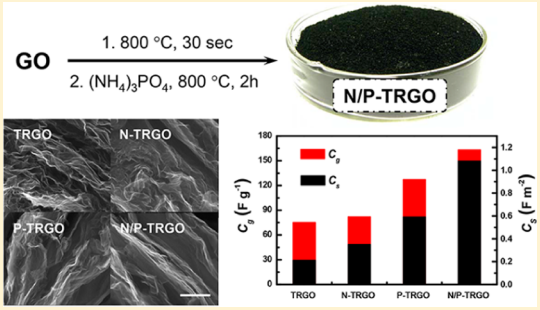

1. INTRODUCTION

The interest in the development of electrochemical capacitors (also called supercapacitors) has been increasing due to their higher power density and longer life cycles than batteries.[1−3] There has been considerable scientific interest in the use of nanostructured carbon materials such as carbon nanotube,[4,5] onion-like carbon,[6,7] graphene,[3,8−12] and carbon nanofiber[13,14] for supercapacitors. Among these, graphene, a monolayer of sp^2 carbon atoms in honeycomb structure, draws extensive scientific and industrial attention due to its high electrical and thermal conductivity, huge specific area, rich surface functional groups, wide electrochemical window, and high chemical stability.[3]

Generally, texture and surface properties are two main factors that affected the supercapacitive performance of graphene relative materials.[3,15−17] Ruoff et al. have first reported the usage of chemically reduced graphene oxide (CRGO) for the electrode materials of supercapacitors.[12] The relative high specific area (705 m^2 g^{-1}) and high heteroatom concentration (C/O = 11.5; C/N = 23) allow these chemically modified graphenes to have excellent supercapacitive performance in both aqueous and organic electrolytes. High specific area graphene relative materials can be synthesized by activations—the most extensively used approaches for the preparation of porous carbons. With KOH activation of microwave-exfoliated graphite oxide (MEGO), Ruoff et al. have prepared a porous carbon with extremely high surface area up to 3100 m^2 g^{-1}.[18] And capacitor cells assembled with the activated MEGO show a high specific capacitance in organic electrolytes. Graphene oxide (GO) can be well dispersed in aqueous solution as individual sheets, but graphene sheets often aggregated and restacked after ether chemical reduction or thermal exfoliation. The agglomeration and the restacking of graphene sheets will not only decrease the surface area of reduced graphene oxide (RGO) but also deter the electrolyte ions from accessing to the surface of RGO sheets.[10] To prevent agglomeration and restacking, self-assembled graphene hydrogel with a novel 3D cross-linked porous structure has been recently reported by Shi's groups.[19] Graphene hydrogel prepared by chemical reduction of GO solution with sodium ascorbate exhibits excellent electrochemical capacitive performance with the specific capacitance up to 240 F g^{-1}. In addition, a novel method through intercalating of spacers (guest) into graphene layers (host) avoiding the agglomeration and irreversible restacking graphene sheets has been developed in the past few years.[20] Metal nanoparticles,[21] metal oxide nanoparticles,[22,23] and nano- or microcarbons (carbon blacks,[24] mesoporous carbon spheres,[25] and carbon nanotubes[26]) can be used as spacers. Those host−guest hybrids show improved electrochemical capacitive performances due to not only larger surface area and the enhanced electrolyte accessibility of electrodes contrast to the host itself but also pseudocapacitance introduced by guest species such as metal or metal oxide nanoparticles.

Surface functionalities, especially oxygen-containing groups, were the other main factor that affected the electrochemical capacitor performance of graphene relative materials.[16] C/O atomic ratios is usually used to characterize the reduce level of

Received: February 14, 2013
Revised: May 16, 2013
Published: June 27, 2013

   dx.doi.org/10.1021/jp4015959 | J. Phys. Chem. C 2013, 117, 14912−14919

RGOs for both chemical reduction and thermal reduction. In most cases for the RGOs that achieved high specific capacitance values, C/O ratios are relative low (<10) depending on the preparation method.[3] The high density of O-containing groups on RGO sheets can not only improve the wettability of electrodes but also contribute to the pseudocapacitance via Faradaic surface reaction. On the other hand, the doping heteroatoms (such as N or B), which can modify the donor−acceptor character of the graphene sheets and consequently contribute to the pseudocapacitance, is an effective approach to enhance the capacitive performance of the RGOs.[27,28] It has been reported that the conductivity of RGOs have an important influence on their capacitive performance, especially the rate performance. The conductivity of RGO depends not only on the reduction level (C/O ratios) but also on factors such as doping concentration, defects, and charge mobility. The reduction level of TRGO can be precisely controlled by the annealing temperature, the duration, and the atmosphere. Defects detrimental to the conductivity are also generated during the thermal treatment. Incorporating of N in the C lattice can significantly enhance the conductivity of graphene. Thermal annealing of GO in the presence of various N precursors (such as urea[29−31] and melamine[32]) seems a practical method for the synthesis of N-doped graphene with high conductivity. Temperature is the principal factor influencing the N and/or O content, owing to the competitive doping nature of N and O.[33,34] However, these N species usually have poor wettablility without the aid of O groups.[3] In this context, a simplified, safe, scalable, and low-cost method to synthesize graphene relative electrode materials with high density of stable surface N/O-containing groups is a highly desired for their application in high performance supercapacitor. Moreover, the understanding of doping effects on the electrochemical properties of RGOs is also urgent at the present time.

Here, we present a very simple and cost efficient approach for the synthesis of the N/P-codoped graphene with high density of thermal stable surface groups through pyrolysis of thermally exfoliated graphene oxide (TEGO) in the presence of the inorganic salt $(NH_4)_3PO_4$. The structure, morphology, and texture properties were characterized by X-ray diffraction (XRD), Raman spectrum, scan electron microscopy (SEM), and N_2 sorption. Surface properties were studied using X-ray photoelectron energy spectrum (XPS). Electrochemical properties were investigated by cyclic voltammetry (CV) and galvanostatic charge−discharge measurements. The influence of N/P codoping on the surface/structural properties and the electrochemical performances were systematically investigated.

2. EXPERIMENTAL SECTION

Preparation of Doped TRGOs. GO was prepared from natural graphite by a modified Hummers' method as described in the literature.[35] Typically, graphite (3 g) was dispersed in a solution of H_2SO_4 containing of 2.5 g of P_2O_5. The mixture was heated to 80 °C and kept for 4 h at this temperature. Then the mixture was cooled to room temperature diluted with 500 mL of water. The preoxidized graphite was filtrated and washed with copious amounts of water and dried at 110 °C overnight. The resulted preoxidized graphite was further oxidized in 120 mL of H_2SO_4 with $KMnO_4$ (15 g). The mixture was first cooled by immersion in an ice bath for 2 h, then removed the ice bath, and further oxidized at room temperature for another 2 h. Finally, the mixture was heated to 90 °C for 2 h and then cooled to room temperature. 900 mL of water was added carefully to keep the temperature below 50 °C, then 20 mL of 30% H_2O_2 was added, and a brilliant yellow suspension was formed. The mixture was left overnight without agitation. The gold yellow GO particles are settled at the bottom of the container, and the black incomplete oxidized particles that floated on the liquid can be easily separated by decantation and discarded. The product was filtrated, washed with 10% wt HCl and then copious amounts of water to remove metal ions and acid, and dried under vacuum at 50 °C for 24 h.

Thermally exfoliated graphene oxide (TEGO, C/O ∼ 11) was prepared by thermally exfoliated of GO at 800 °C for 30 s under a N_2 atmosphere. Doped TRGO (N-TRGO, P-TRGO, N/P-TRGO) was prepared by thermal annealing of TEGO at high temperature in the presence of additives NH_4Cl, H_3PO_4, or $(NH_4)_3PO_4$ under an inert atmosphere. The solid inorganic salt (2 g), such as NH_4Cl and $(NH_4)_3PO_4$, was ground into fine powder and physically mixed with 1 g of ERGO powder; for the liquid precursor, 1 g of ERGO powder was simply dipped into 2 g of concentrated H_3PO_4. The mixture was then transferred to a quartz boat and thermally annealed at 800 °C for 2 h under a N_2 atmosphere. The product was collected and washed with copious amounts of hot water to remove any impurities and then dried at 110 °C overnight. TRGO was prepared by thermally treated of TEGO at the same conditions without using of any additive.

Characterization of Samples. XRD patterns were collected on a Rigaku D/Max2400 diffractometer equipped with Cu Kα radiation (40 kV, 100 mA). N_2 sorption measurements were performed at 77 K with a Quantachrome adsorption instrument. Prior to the measurements, the samples were degassed at 150 °C for 4 h. The elemental analysis (EA) was done by a conventional CHN combustion method (Vario EL-3) based on the burn-off of the sample and TCD analysis of N mass percentage. X-ray photoelectron spectroscopy (XPS, ESCALAB250, Thermo VG Corporation) was used in the surface analyses of the samples. The Al Kα line (15 kV, 10 mA, 150 W) was used as a radiation source, and the C 1s peak position was set at 284.6 eV as an internal standard. The peak separations of the N 1s and O 1s core level peaks were estimated by least-squares with Gaussian−Lorentzian functions after subtraction of background noise. The concentration of each element was calculated from the area of the corresponding peak calibrated with the atomic sensitivity factor using C as the reference. SEM investigations were carried out on a FEI Nova NanoSEM 450. The electrical conductivity of samples were measured on a four-point resistivity measurement system (RST-9, China).

Electrochemical Measurement. The capacitor electrodes with a diameter of 10 mm were obtained by pressing a mixture of the samples (80 wt %), carbon black (10 wt %), and polytetrafluoroethylene (PTFE) (10 wt %) onto the foam nickel collector. The CV tests and electrochemical impedance spectroscopy (EIS) were conducted using an electrochemical working station (CHI 660D, Shanghai, China) in a three-electrode cell system, employing a platinum foil as the counter electrode and Hg/HgO as the reference electrode. CVs were recorded between −0.9 and −0.1 V at different scanning rates. The galvanostatic charge−discharge measurements were conducted on a battery testing system (Land CT 2001, Wuhan, China). The tests were performed in the potential range of −0.9 to −0.1 V at different current densities by a three-electrode system. The specific capacitances (C_g) were

dx.doi.org/10.1021/jp4015959 | J. Phys. Chem. C 2013, 117, 14912−14919

calculated from discharge curves according the equation $C_g = I\Delta t/m\Delta V$, where I (A) is the discharge current, Δt (s) is the discharge time, m (g) is the mass of the active carbon material of the single electrode (working electrode), and ΔV (V) is the potential difference during the discharge. All electrochemical experiments were carried out in an aqueous solution of 6 M KOH at room temperature.

3. RESULTS AND DISCUSSION

The XRD pattern of pristine graphite, GO, and TRGO is shown in Figure 1. The diffraction peaks associated with

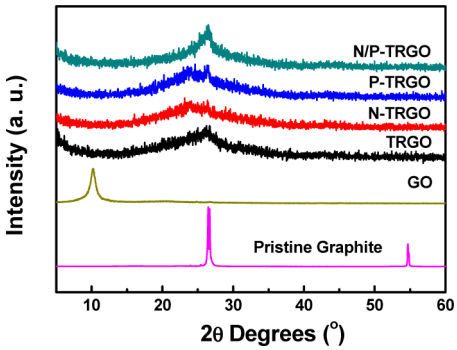

Figure 1. XRD pattern of pristine graphite, GO, TRGO, and doped TRGOs.

graphite at 2θ of 26° disappeared after chemical oxidized with $KMnO_4$, indicating the complete oxidation of the pristine graphite, and a new diffraction peak at 11° appears, suggesting the progress of intercalation of the pristine graphite. The graphene oxides after thermally reduced give broad peaks centered at about 24°−26°, indicating the restacking of graphene sheets. In addition, N/P-TRGO shows a more resolved peak (with a shift toward more higher angle up to 26°) compared with TRGO, N-TRGO, and P-TRGO, suggesting a higher restacking level. The doping of heteroatoms and the higher restacking level led to a significant improvement in electronic conductivity of N-, P-, or N/P-doped TRGO (Table 1). N-TRGO with the highest N content and relatively low O content exhibits the highest conductivity.

Figure 2 shows the SEM images of TRGO. Typical aggregates of wrinkled layered structures are observed for all samples with only a slightly trend toward higher level of overlapping by heteroatom-doping (smoother and flatter planes can be seen in the SEM images (Figure 2b−d)).[36] These results indicate that N and/or P precursor has little influence on the morphology of the resulting TRGO, and there still remains quantities of macropores for electrolyte ions can access after thermal annealing and/or doping.

The N_2 sorption is further employed to characterize the pore structure of doped TRGOs. TRGOs both doped and undoped exhibit type II isotherms with typical H3 hysteresis loops, which

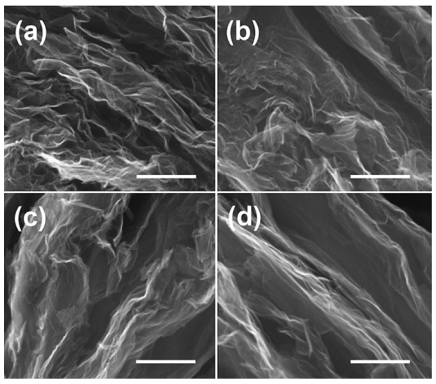

Figure 2. SEM images for (a) TRGO, (b) N-TRGO, (c) P-TRGO, and (d) N/P-TRGO with the scale bar of 1 μm.

were the characteristic of random aggregated plate-like solid with slit-shaped pores.[37] The BET surface area (S_{BET}) and pore volume of TRGOs decrease after heteroatom doping, from 355 $m^2\ g^{-1}$ for TRGO to 234 and 215 $m^2\ g^{-1}$ for N-TRGO and P-TRGO, and then decreased to only 152 $m^2\ g^{-1}$ for N/P-TRGO, the pore volume decreased correspondingly. According to the pore development mechanism of TRGO, the decrease of the surface area during the thermal annealing process when doping is attributed to the restacking, partial overlapping, and coalescing of the graphene sheets.[38] The pore size distribution (PSD) plots of all the samples show a peak at ~2 nm. Among them, TRGO exhibits a much broader PSD with a tail toward larger pore size direction, and the doped samples show the narrower peaks, which indicates that the diminishing of the large pores during the doping process. These results are consent to the XRD, SEM, and S_{BET} data.

Raman spectroscopy is carried out to investigate the structural differences of samples. Two typical peaks centered at about 1350 cm^{-1} (D line) and 1590 cm^{-1} (G line) are resolved for all samples (Figure 4), which associated with the E_{2g} phonon of sp^2 C atoms and breathing mode of k point of phonos of A_{1g} symmetry, respectively. The significant increase of D line and the shift of G line toward a higher wavenumber compared with pristine graphite indicate that the decrease of the in-plane domain of sp^2 carbon lattice due to the oxidation and the presence of the defects and disorder structures in the TRGOs. Generally, the I_D/I_G ratio is used to evaluate the disorder in the graphene derivates. The I_D/I_G ratios of doped TRGO are slightly higher than that of TRGO, suggesting a higher disorder level due to the generating of smaller nanocrystalline graphene domains by heteroatom doping.[39]

To investigate the surface composition of TRGO and doped TRGO, XPS was preformed. The surface N contents for N-TRGO and N/P-TRGO was found to be 4.4 and 3.4 at. %, respectively (Table 1). The surface P contents of P-TRGO and N/P-TRGO was 3.4 and 4.3 at. %, respectively. For TRGOs, C/O atomic ratios are strongly affected by the reduction

Table 1. XPS Elemental Analysis (at. %), Specific Surface Area, and Electrical Conductivity of Samples

samples	C	N	O	P	atomic ratio of C/O	S_{BET} ($m^2\ g^{-1}$)	electrical conductivity (S m^{-1})
GO	70.7	0.2	29.1		2.4		0.01
TRGO	95.6		4.4		21.7	355	124
N-TRGO	88.9	3.2	7.8		11.4	234	820
P-TRGO	86.7		9.8	3.4	8.8	215	290
N/P-TRGO	79.3	2.9	13.4	4.3	5.9	152	575

dx.doi.org/10.1021/jp4015959 | J. Phys. Chem. C 2013, 117, 14912−14919

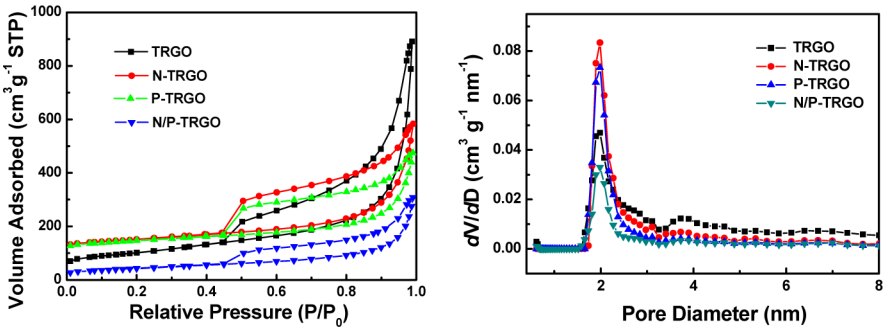

Figure 3. (a) N_2 sorption isotherms and (b) pore size distributions of TRGO and doped TRGOs.

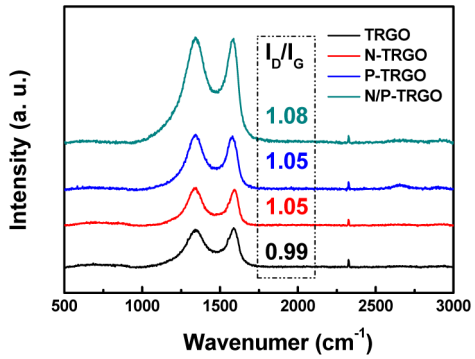

Figure 4. Raman spectra (λ_{ex} = 532 nm) of TRGO and doped TRGO; I_D/I_G (intensity ratio of D-bands to G-bands) values are also shown for each spectrum.

temperature, time, and atmosphere.[3,38,40] The C/O atomic ratio of TRGO was 21.7, indicating the high level of the reduction; C/O decreased after heteroatom doping, suggesting the reduction process was inhibited.

The high-resolution C 1s peaks for all samples are centered at 284.6 eV with a tail toward higher binding energy. C 1s (Figure 5a) spectra for TRGO and P-TRGO can be

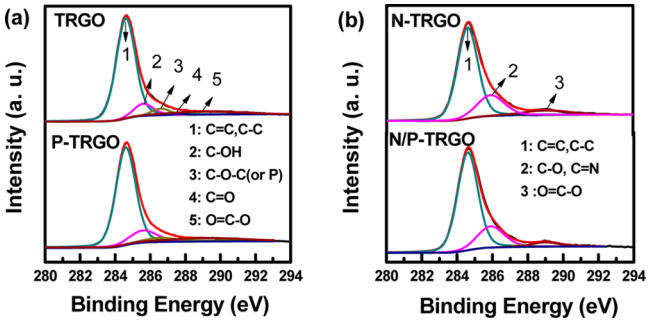

Figure 5. C 1s XPS spectra for (a) TRGO and P-TRGO; (b) N-TRGO and N/P-TRGO.

deconvolved into five components, namely, C=C (sp^2), C–OH, C–O–C (or P), C=O, and O=C–O. For N-doping samples N-TRGO and N/P-TRGO (Figure 5b), three peaks were fitted by the deconvolution of the C 1s spectra as follows: C=C (sp^2), C–O (and/or C=N), and O=C–O. The peak corresponding to C–P bonding (between graphitic and aliphatic carbons) cannot be resolved.[41] The fitting of the N 1s spectra can be resolved into four individual component peaks representing N-6 (398.5 eV), N-5 (400.0 eV), N-Q (401.2 eV), and N-X (403.0 eV) groups (Figure 6a). It should

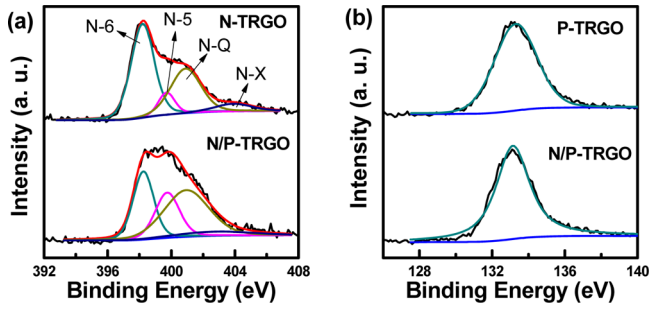

Figure 6. (a) N 1s XPS spectra for N-TRGO and N/P-TRGO and (b) P 2p XPS spectra for P-TRGO and N/P-TRGO.

be stressed here N-6 and N-Q peaks do not just correspond to pyridinic and quaternary N but also to P=N and P–N bonds.[41] The peak deconvolution analysis of N 1s and O 1s core level were summarized in Table 2. It is worth noting that

Table 2. Fitted Results of O 1s and N 1s Core Level XPS Spectra of TRGO and Doped TRGOs

samples	I1	I2	I3	N-6	N-5	N-Q	N-X
TRGO	15.1	34.5	50.4				
N-TRGO	14.7	21.5	63.8	52.0	8.8	32.5	6.7
P-TRGO	20.4	55.0	24.6				
N/P-TRGO	31.7	43.1	25.2	28.6	22.4	42.6	6.4

the contribution of N-5 (pyrrolic and pyridone) species of N/P-TRGO are much higher than that of N-TRGO. For P-containing TRGOs, peaks at about 133 eV can be attributed to (pyro)phosphates (tetrahedral PO_4 species) and/or (pyro)-phosphonate ($C-PO_3$) groups (Figure 6b), and the O/P atomic ratio of P-related samples is ~3. That means most of O atoms are P-related.

The O 1s spectra in Figure 7 indicate that the I4 species (carboxylic acid groups and/or chemisorbed/intercalated adsorbed water molecules) at the higher binding energy (534.7 eV) can hardly be resolved for all samples.[40] Therefore, O 1s spectra of TRGO and doped TRGO can be deconvoluted into three main peaks around 531.1, 532.1, and 533.4 eV according to previous study, which can be assigned to C=O or P=O (I1), aliphatic C–O or P–O (I2), and aromatic C–O (I3), respectively. The contribution of I1, which was generally considered as pseudocapacitive activate, for P-containing samples is much higher than those for P-free samples (Tables 1 and 2). Ganguly et al. have reported the detailed investigation of the development of surface groups on the GOs during the thermal reduction.[40] At low temperature (<200 °C), the most

dx.doi.org/10.1021/jp4015959 | J. Phys. Chem. C 2013, 117, 14912–14919

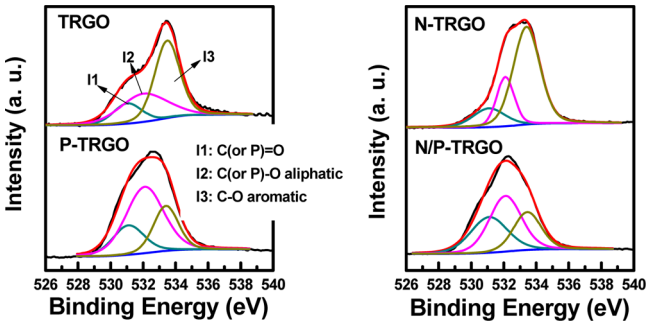

Figure 7. O 1s XPS spectra for doped TRGOs.

prominent peak was I2, but the relative intensity of the I3 peak overtook that of I2 when temperature was raised to 400 °C. In this work, for P-free samples (TRGO and N-TRGO), the dominant O groups that stable at high temperature (>400 °C) are aromatic C−O (I3), which was consistent with Ganguly's results. Most of the basal plane aliphatic C−O (I2) groups can be removed at a low temperature due to the thermal restoration of the aromatic graphitic structure. Interestingly, for P-containing samples, I2 configurations (singly bonded to aliphatic carbons) became the most predominant peak, which indicated that the P-doping stunted the recovery of graphitic lattice during their thermal reduction (Table 2).

There are three possible P-related O groups (P═O, P−O−$C_{aliphatic}$, and P−O−$C_{aromatic}$) according to XPS analysis. Given the poor thermal stability of C−O−$C_{aliphatic}$, the high proportion of I2 for P-doped TRGO suggests a higher contribution of P−O−$C_{aliphatic}$.[37,40] P−O−$C_{aliphatic}$ and P−O−$C_{aromatic}$ groups can also be detected by FTIR spectra (Figure S1). The peak at ∼1190 cm^{-1} can be assigned to the stretching vibration of P═O and P−O−$C_{aromatic}$; the should peak at ∼1175 cm^{-1} can be assigned to the stretching vibration of P−O−$C_{aliphatic}$. And the proposed configurations of these groups are shown in Scheme 1. For the basal plane configuration, the π conjugation of the graphitic network must be broken due to the formation of the out-of-plane P−O−$C_{aliphatic}$ σ bonds in the (pyro)phosphonate and/or (pyro)phosphonate ester structure.

Scheme 1. Proposed Structural Model for P-Containing Groups on P-Doped TRGO

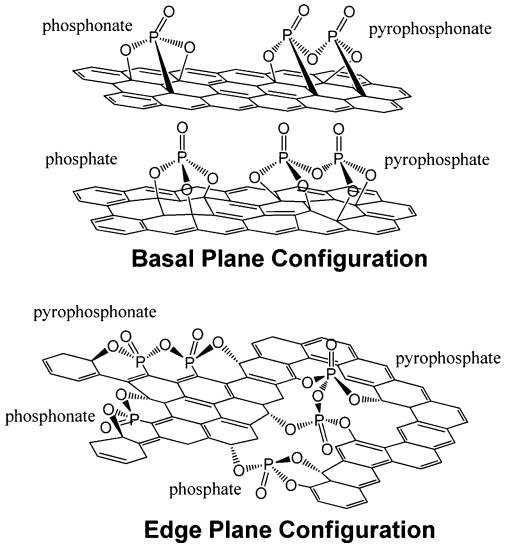

Moreover, the concentrations of in-plane O atom for P-doped TRGO are much higher than those of TRGO and N-TRGO (Table 1). Thus, structures will significantly increase the O coverage on the basal plane of P-doped graphene nanosheets. (Pyro)phosphonate and/or (pyro)phosphonate groups can also locate at the edge defect sites. Because of the tetrahedral configuration of P center atom, the aromatic planar structure must be distorted at these defects, as shown in Scheme 1. However, the domains of these defects both on the basal plane and/or at the edge sites must be very local because P-doped samples exhibit the higher restacking level graphitic network according to the XRD, N_2 sorption, and SEM results. In other words, these defects must have no obvious influence on the long-range structure of the P-doped TRGO.

Figure 8a,b shows the CV plots with sweep rates of 5 and 100 mV s^{-1} for all samples. All of the TRGOs show better

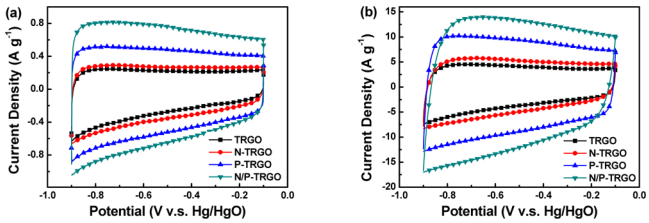

Figure 8. Evolution of CVs at (a) 5 and (b) 100 mV s^{-1} for TRGO and doped TRGOs.

symmetrical rectangular shape for CV curves than those of CRGOs at both low and high sweep rate.[2,3] And the doped TRGO samples exhibit higher current values of CV, indicating the capacitive behavior of TRGO can be improved by heteroatom doping. In addition, the codoped sample N/P-TRGO has the largest area of in CV plots.

In order to evaluate the contribution of heteroatom doping, the surface-normalized specific capacitance ($C_s = C_g/S_{BET}$) was employed (Figure 9a). N-TRGO and P-TRGO showed the

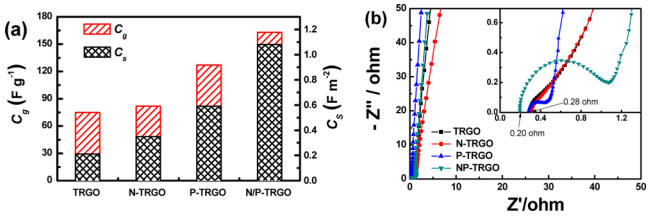

Figure 9. (a) Plot of gravimetric specific capacitance (C_g, F g^{-1}) and surface-normalized specific capacitance (C_s, F m^2) for TRGOs at a current density of 100 mA g^{-1}. (b) Nyquist impedance spectra of TRGO and doped TRGOs (inset shows an expanded view for high-frequency range).

improved C_s compared with TRGO. Both the highest C_g value of 165 F g^{-1} and C_s value of 1.08 F m^2 were obtained for N/P-TRGO, which were much higher than those of the TRGO (C_g = 75 F g^{-1} and C_s = 0.211 F m^2) obtained under the same condition and also higher than those of others reported.[15,37] Generally, surface area and O content in RGOs are crucial to their supercapacitive performance. It has been reported the C_g of thermally reduced GO decreased drastically when reduced at a higher temperature (>400 °C) due to the decrease of S_{BET} and the intensive removal of O-containing groups.[15] It was also reported N-doping can improve the pseudocapacitive perform-

dx.doi.org/10.1021/jp4015959 | J. Phys. Chem. C 2013, 117, 14912−14919

ance of RGOs.[42] In this work, the S_{BET} of N/P-TRGO is rather low (152 m^2 g^{-1}), so the high C_g and C_s values should be attributed to the N doping and its extremely high O content (13.4 at. %). In addition, the doping effects of P and N on the structure and electrochemical performance are different. Mono-N-doping can lower the C/O ratio of TRGO, but the S_{BET} decreased also. Given the N doping usually occurs at the defects and/or the edges of graphene sheets, partial of the high temperature stable N configurations are unaccessible to electrolyte due to the aggregation and their poor wettability.[27,33,42] Thus, a slight increase (from 75 F g^{-1} for TRGO to 82 F g^{-1} for N-TRGO) in C_g is observed for mono-N-doping. P-doping can greatly improve the surface O content, and N/P-TRGO exhibits an extreme low C/O ratio of about 6. Mono-P-doping is found to be more effective than mono-N-doping in the capacitive performance with much higher C_g and C_s values. Similar to mono-N-doping, mono-P-doping can also decrease the S_{BET}, which was detrimental to EDLCs performance. But the high O coverage and the distortion of the graphene lattice induced by tetrahedral configuration of P atom may facilitate the accessibility of electrolyte ions. The unreachable N-active sites because of poor wetting properties can regain their pseudocapacitance when codoped with P. Combination of these two effects, N/P-TRGO exhibits the best supercapacitive performance, and the significant enhancement in both C_g and C_s can be attributed to the pseudocapacitive effect induced by codoping of N and P.

Figure 9b shows the Nyquist plots of TRGO and doped TRGOs electrodes. All samples displayed two parts including a semicircle in the high frequency range and a slope line in the low frequency range. N-TRGO exhibited a more inclined curve at low frequency region, indicating a higher contribution of pseudocapacitance. P-TRGO exhibited a more vertical line at low frequency region, indicating a higher contribution of EDLCs. The intersection of the high frequency region at the *x*-axis corresponds to the equivalent series resistance (ERS) of electrode. NP-TRGO shows a low ESR (0.2 ohm), which could ascribed to the high wettability of the electrode surface.

It is well-known that the surface properties of activated carbons are strongly depended on the annealing temperature. For the supercapacitor application, the surface oxygen-containing groups can not only improve the wettability properties of electrodes toward electrolytes but also contribute to the capacitance via pseudocapacitance.[43] However, not all of oxygen-containing groups are benefit to the electrochemical capacitive performances. For example, carboxy-type groups (−COOH, carboxylic acid; −(C═O)−O−(C═O)−, carboxylic anhydrides; and −C═O−O, lactones) were believed to harmful to the electrochemical capacitive properties of porous carbons.[44,45] TPD experiments have illustrated that carboxylic acid, carboxylic anhydrides, and lactones in GO are decomposed at 220−300, 350−450, and 500−700 °C, respectively.[15,38,40,46,47] Thus, thermal treatment at a high temperature may be the most effective way to remove these unstable groups. In this work, high rate performances with capacitance retention ratio >80% were achieved for all samples, as shown in Figure 10a. Figure 10b shows the performance of supercapacitor in two electrode configuration over 2000 charge−discharge cycles at 500 mA g^{-1}. The capacitance retention ratio of TRGO, N-TRGO, P-TRGO, and N/P-TRGO are 91, 84, 86, and 91%, respectively.[25] For traditional carbon electrode materials such as activated carbons, the presence of thermal unstable O groups often led to a poor cycle life.[45,48−50] But for some case of graphene relative electrode materials especially chemically reduced GOs with large quantity of thermal unstable groups, the capacitance does not degrade but increases upon cycle.[51] Such anomalous cycle stability can be attributed to the redox of the residual O groups. The capacitive properties can be improved continuously during the cycling measurements, but this process is irreversible.[50] For thermally reduced GO and the most of carbon electrode materials, thermal elimination of unstable groups at high temperature is an effective method to improve the rate performance and the cycle stability.[37,48] Herein to eliminate those groups completely, we treated the TEGO with dopants at 800 °C for as long as 2 h, so a better rate capability and cycle performance have been obtained.

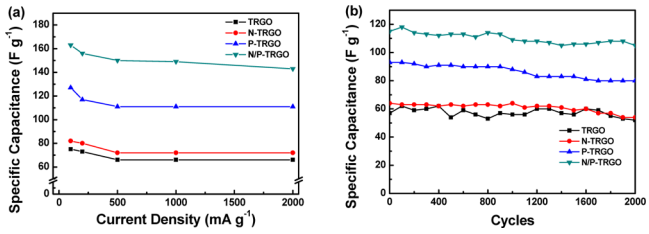

Figure 10. (a) Specific capacitance curves of TRGO and doped TRGOs at different current density and (b) specific capacitance of TRGO and doped TRGOs within first 2000 cycles at the current density of 500 mA g^{-1}.

4. CONCLUSION

N/P-TRGO was prepared by thermal annealing of TEGO in the presence of inorganic salt $(NH_4)_3PO_4$. N/P-TRGO is aggregates of crumpled sheets with low surface area. P-doping greatly improved the surface O concentration of N/P-TRGO. The high temperature and long period of heat treatment can eliminate the unstable groups on TRGO sheets. Electrochemical tests showed that the best performance was obtained for N/P-TRGO with specific capacitance of 165 F g^{-1} and high capacitance retention ratio of >80%. The high electrochemical capacitive performance can be ascribed to the rich and accessible thermal stable heteroatom-containing groups induced by N and P codoping. This investigation demonstrates that N and P codoping is an effective method to enhance the electrochemical performance of TRGOs. Since there are still lots of options to increase the S_{BET} of the codoped graphene, the electrochemical capacitive performance of N/P-TRGO will be further improved.

■ ASSOCIATED CONTENT

Supporting Information

FTIR spectra of P-TRGO and N/P-TRGO. This material is available free of charge via the Internet at http://pubs.acs.org.

■ AUTHOR INFORMATION

Corresponding Author

*Fax +86-411-84986080; e-mail jqiu@dlut.edu.cn (J.Q.).

Notes

The authors declare no competing financial interest.

■ ACKNOWLEDGMENTS

This work was supported by the National Natural Science Foundation of China (No. 21003016, 21276045) and China Postdoctoral Science Foundation (No. 20100481227).

REFERENCES

(1) Ghosh, A.; Lee, Y. H. Carbon-Based Electrochemical Capacitors. *ChemSusChem* **2012**, *5*, 480−499.

(2) Bose, S.; Kuila, T.; Mishra, A. K.; Rajasekar, R.; Kim, N. H.; Lee, J. H. Carbon-Based Nanostructured Materials and Their Composites As Supercapacitor Electrodes. *J. Mater. Chem.* **2012**, *22*, 767−784.

(3) Huang, Y.; Liang, J.; Chen, Y. An Overview of the Applications of Graphene-Based Materials in Supercapacitors. *Small* **2012**, *8*, 1805−1834.

(4) Niu, C. M.; Sichel, E. K.; Hoch, R.; Moy, D.; Tennent, H. High Power Electrochemical Capacitors Based on Carbon Nanotube Electrodes. *Appl. Phys. Lett.* **1997**, *70*, 1480−1482.

(5) Chen, J. H.; Li, W. Z.; Wang, D. Z.; Yang, S. X.; Wen, J. G.; Ren, Z. F. Electrochemical Characterization of Carbon Nanotubes As Electrode in Electrochemical Double-Layer Capacitors. *Carbon* **2002**, *40*, 1193−1197.

(6) Portet, C.; Yushin, G.; Gogotsi, Y. Electrochemical Performance of Carbon Onions, Nanodiamonds, Carbon Black and Multiwalled Nanotubes in Electrical Double Layer Capacitors. *Carbon* **2007**, *45*, 2511−2518.

(7) Borgohain, R.; Li, J.; Selegue, J. P.; Cheng, Y. T. Electrochemical Study of Functionalized Carbon Nano-Onions for High-Performance Supercapacitor Electrodes. *J. Phys. Chem. C* **2012**, *116*, 15068−15075.

(8) Zhang, L. L.; Zhou, R.; Zhao, X. S. Graphene-Based Materials As Supercapacitor Electrodes. *J. Mater. Chem.* **2010**, *20*, 5983−5992.

(9) Lin, Z.; Liu, Y.; Yao, Y.; Hildreth, O. J.; Li, Z.; Moon, K.; Wong, C.-p. Superior Capacitance of Functionalized Graphene. *J. Phys. Chem. C* **2011**, *115*, 7120−7125.

(10) Wang, Y.; Shi, Z.; Huang, Y.; Ma, Y.; Wang, C.; Chen, M.; Chen, Y. Supercapacitor Devices Based on Graphene Materials. *J. Phys. Chem. C* **2009**, *113*, 13103−13107.

(11) Liu, C.; Yu, Z.; Neff, D.; Zhamu, A.; Jang, B. Z. Graphene-Based Supercapacitor with an Ultrahigh Energy Density. *Nano Lett.* **2010**, *10*, 4863−4868.

(12) Stoller, M. D.; Park, S.; Zhu, Y.; An, J.; Ruoff, R. S. Graphene-Based Ultracapacitors. *Nano Lett.* **2008**, *8*, 3498−3502.

(13) Kim, C.; Yang, K. S. Electrochemical Properties of Carbon Nanofiber Web As an Electrode for Supercapacitor Prepared by Electrospinning. *Appl. Phys. Lett.* **2003**, *83*, 1216−1218.

(14) Kim, S. U.; Lee, K. H. Carbon Nanofiber Composites for the Electrodes of Electrochemical Capacitors. *Chem. Phys. Lett.* **2004**, *400*, 253−257.

(15) Zhao, B.; Liu, P.; Jiang, Y.; Pan, D.; Tao, H.; Song, J.; Fang, T.; Xu, W. Supercapacitor Performances of Thermally Reduced Graphene Oxide. *J. Power Sources* **2012**, *198*, 423−427.

(16) Deng, W.; Ji, X.; Gomez-Mingot, M.; Lu, F.; Chen, Q.; Banks, C. E. Graphene Electrochemical Supercapacitors: the Influence of Oxygen Functional Groups. *Chem. Commun.* **2012**, *48*, 2770−2772.

(17) Wang, Y.; Wu, Y.; Huang, Y.; Zhang, F.; Yang, X.; Ma, Y.; Chen, Y. Preventing Graphene Sheets from Restacking for High-Capacitance Performance. *J. Phys. Chem. C* **2011**, *115*, 23192−23197.

(18) Zhu, Y.; Murali, S.; Stoller, M. D.; Ganesh, K. J.; Cai, W.; Ferreira, P. J.; Pirkle, A.; Wallace, R. M.; Cychosz, K. A.; Thommes, M. Carbon-Based Supercapacitors Produced by Activation of Graphene. *Science* **2011**, *332*, 1537−1541.

(19) Xu, Y.; Sheng, K.; Li, C.; Shi, G. Self-Assembled Graphene Hydrogel via a One-Step Hydrothermal Process. *ACS Nano* **2010**, *4*, 4324−4330.

(20) Lin, J.; Zhong, J.; Bao, D.; Reiber-Kyle, J.; Wang, W. Supercapacitors Based on Pillared Graphene Nanostructures. *J. Nanosci. Nanotechnol.* **2012**, *12*, 1770−1775.

(21) Si, Y.; Samulski, E. T. Exfoliated Graphene Separated by Platinum Nanoparticles. *Chem. Mater.* **2008**, *20*, 6792−6797.

(22) Wu, Z.-S.; Wang, D.-W.; Ren, W.; Zhao, J.; Zhou, G.; Li, F.; Cheng, H.-M. Anchoring Hydrous RuO_2 on Graphene Sheets for High-Performance Electrochemical Capacitors. *Adv. Funct. Mater.* **2010**, *20*, 3595−3602.

(23) Mishra, A. K.; Ramaprabhu, S. Functionalized Graphene-Based Nanocomposites for Supercapacitor Application. *J. Phys. Chem. C* **2011**, *115*, 14006−14013.

(24) Yan, J.; Wei, T.; Shao, B.; Ma, F.; Fan, Z.; Zhang, M.; Zheng, C.; Shang, Y.; Qian, W.; Wei, F. Electrochemical Properties of Graphene Nanosheet/Carbon Black Composites As Electrodes for Supercapacitors. *Carbon* **2010**, *48*, 1731−1737.

(25) Lei, Z.; Christov, N.; Zhao, X. S. Intercalation of Mesoporous Carbon Spheres between Reduced Graphene Oxide Sheets for Preparing High-Rate Supercapacitor Electrodes. *Energy Environ. Sci.* **2011**, *4*, 1866−1873.

(26) Qiu, L.; Yang, X.; Gou, X.; Yang, W.; Ma, Z.-F.; Wallace, G. G.; Li, D. Dispersing Carbon Nanotubes with Graphene Oxide in Water and Synergistic Effects between Graphene Derivatives. *Chem.—Eur. J.* **2010**, *16*, 10653−10658.

(27) Jeong, H. M.; Lee, J. W.; Shin, W. H.; Choi, Y. J.; Shin, H. J.; Kang, J. K.; Choi, J. W. Nitrogen-Doped Graphene for High-Performance Ultracapacitors and the Importance of Nitrogen-Doped Sites at Basal Planes. *Nano Lett.* **2011**, *11*, 2472−2477.

(28) Li, X. L.; Wang, H. L.; Robinson, J. T.; Sanchez, H.; Diankov, G.; Dai, H. J. Simultaneous Nitrogen Doping and Reduction of Graphene Oxide. *J. Am. Chem. Soc.* **2009**, *131*, 15939−15944.

(29) Su, P.; Guo, H.-L.; Peng, S.; Ning, S.-K. Preparation of Nitrogen-Doped Graphene and Its Supercapacitive Properties. *Acta Phys.-Chim. Sin.* **2012**, *28*, 2745−2753.

(30) Lin, Z.; Waller, G.; Liu, Y.; Liu, M.; Wong, C.-P. Facile Synthesis of Nitrogen-Doped Graphene via Pyrolysis of Graphene Oxide and Urea, and Its Electrocatalytic Activity toward the Oxygen-Reduction Reaction. *Adv. Energy Mater.* **2012**, *2*, 884−888.

(31) Mou, Z.; Chen, X.; Du, Y.; Wang, X.; Yang, P.; Wang, S. Forming Mechanism of Nitrogen Doped Graphene Prepared by Thermal Solid-State Reaction of Graphite Oxide and Urea. *Appl. Surf. Sci.* **2011**, *258*, 1704−1710.

(32) Sheng, Z. H.; Shao, L.; Chen, J. J.; Bao, W. J.; Wang, F. B.; Xia, X. H. Catalyst-Free Synthesis of Nitrogen-Doped Graphene via Thermal Annealing Graphite Oxide with Melamine and Its Excellent Electrocatalysis. *ACS Nano* **2011**, *5*, 4350−4358.

(33) Huan, T. N.; Khai, T. V.; Kang, Y.; Shim, K. B.; Chung, H. Enhancement of Quaternary Nitrogen Doping of Graphene Oxide via Chemical Reduction Prior to Thermal Annealing and an Investigation of Its Electrochemical Properties. *J. Mater. Chem.* **2012**, *22*, 14756−14762.

(34) Kumar, A.; Ganguly, A.; Papakonstantinou, P. Thermal Stability Study of Nitrogen Functionalities in a Graphene Network. *J. Phys.: Condens. Matter* **2012**, 24.

(35) Kovtyukhova, N. I.; Ollivier, P. J.; Martin, B. R.; Mallouk, T. E.; Chizhik, S. A.; Buzaneva, E. V.; Gorchinskiy, A. D. Layer-by-Layer Assembly of Ultrathin Composite Films from Micron-Sized Graphite Oxide Sheets and Polycations. *Chem. Mater.* **1999**, *11*, 771−778.

(36) Yan, J.; Liu, J.; Fan, Z.; Wei, T.; Zhang, L. High-Performance Supercapacitor Electrodes Based on Highly Corrugated Graphene Sheets. *Carbon* **2012**, *50*, 2179−2188.

(37) Zhang, H.; Bhat, V. V.; Gallego, N. C.; Contescu, C. I. Thermal Treatment Effects on Charge Storage Performance of Graphene-Based Materials for Supercapacitors. *ACS Appl. Mater. Interfaces* **2012**, *4*, 3239−3246.

(38) Ju, H.-M.; Huh, S. H.; Choi, S.-H.; Lee, H.-L. Structures of Thermally and Chemically Reduced Graphene. *Mater. Lett.* **2010**, *64*, 357−360.

(39) Pimenta, M. A.; Dresselhaus, G.; Dresselhaus, M. S.; Cancado, L. G.; Jorio, A.; Saito, R. Studying Disorder in Graphite-Based Systems by Raman Spectroscopy. *Phys. Chem. Chem. Phys.* **2007**, *9*, 1276−1291.

(40) Ganguly, A.; Sharma, S.; Papakonstantinou, P.; Hamilton, J. Probing the Thermal Deoxygenation of Graphene Oxide Using High-Resolution In Situ X-ray-Based Spectroscopies. *J. Phys. Chem. C* **2011**, *115*, 17009−17019.

(41) Hulicova-Jurcakova, D.; Seredych, M.; Lu, G. Q.; Kodiweera, N. K. A. C.; Stallworth, P. E.; Greenbaum, S.; Bandosz, T. J. Effect of Surface Phosphorus Functionalities of Activated Carbons Containing

Oxygen and Nitrogen on Electrochemical Capacitance. *Carbon* **2009**, *47*, 1576−1584.
(42) Wang, H.; Maiyalagan, T.; Wang, X. Review on Recent Progress in Nitrogen-Doped Graphene: Synthesis, Characterization, and Its Potential Applications. *ACS Catal.* **2012**, *2*, 781−794.
(43) Pandolfo, A. G.; Hollenkamp, A. F. Carbon Properties and Their Role in Supercapacitors. *J. Power Sources* **2006**, *157*, 11−27.
(44) Yoshida, A.; Tanahashi, I.; Nishino, A. Effect of Concentration of Surface Acidic Functional Groups on Electric Double-Layer Properties of Activated Carbon Fibers. *Carbon* **1990**, *28*, 611−615.
(45) Hsieh, C.-T.; Teng, H. Influence of Oxygen Treatment on Electric Double-Layer Capacitance of Activated Carbon Fabrics. *Carbon* **2002**, *40*, 667−674.
(46) Cao, J.; Qi, G.-Q.; Ke, K.; Luo, Y.; Yang, W.; Xie, B.-H.; Yang, M.-B. Effect of Temperature and Time on the Exfoliation and Deoxygenation of Graphite Oxide by Thermal Reduction. *J. Mater. Sci.* **2012**, *47*, 5097−5105.
(47) Ye, J.; Zhang, H.; Chen, Y.; Cheng, Z.; Hu, L.; Ran, Q. Supercapacitors Based on Low-Temperature Partially Exfoliated and Reduced Graphite Oxide. *J. Power Sources* **2012**, *212*, 105−110.
(48) Ruiz, V.; Blanco, C.; Granda, M.; Santamaría, R. Enhanced Life-Cycle Supercapacitors by Thermal Treatment of Mesophase-Derived Activated Carbons. *Electrochim. Acta* **2008**, *54*, 305−310.
(49) Bleda-Martínez, M. J.; Lozano-Castelló, D.; Morallón, E.; Cazorla-Amorós, D.; Linares-Solano, A. Chemical and Electrochemical Characterization of Porous Carbon Materials. *Carbon* **2006**, *44*, 2642−2651.
(50) Oda, H.; Yamashita, A.; Minoura, S.; Okamoto, M.; Morimoto, T. Modification of the Oxygen-Containing Functional Group on Activated Carbon Fiber in Electrodes of an Electric Double-Layer Capacitor. *J. Power Sources* **2006**, *158*, 1510−1516.
(51) Chen, Y.; Zhang, X.; Zhang, D.; Yu, P.; Ma, Y. High Performance Supercapacitors Based on Reduced Graphene Oxide in Aqueous and Ionic Liquid Electrolytes. *Carbon* **2011**, *49*, 573−580.